INSTITUTE OF PHYSICS PUBLISHING JOURNAL OF OPTICS A: PURE AND APPLIED OPTICS
J. Opt. A: Pure Appl. Opt. **3** (2001) 429–439 PII: S1464-4258(01)27426-1

UV-induced stress field during Bragg grating inscription in optical fibres

Farid Kherbouche and Bertrand Poumellec[1]

Laboratoire Physico-Chimie de l'Etat Solide, UMR8648 CNRS-UPS, Bât. 414,
Université Paris Sud, 91405 Orsay, France

E-mail: Bertrand.Poumellec@lpces.u-psud.fr

Received 31 July 2001
Published 6 September 2001
Online at stacks.iop.org/JOptA/3/429

Abstract
The present work deals with computation of the stress field caused by UV-induced densification in optical fibre cores during Bragg grating elaboration. The stress field is calculated using the finite element method and leads to a contribution to the refractive index modulation being perpendicular to the direction of propagation. The birefringence associated with the stress field is evaluated. Another important result is the growth of a shear stress component developed during Bragg grating writing. This can contribute to the fragilization of fibres. We suggest that these shear stresses are involved in the triggering of a refractive index contribution opposite to the one of the densification which is a negative one associated with the so-called type IIA Bragg grating.

Keywords: Bragg gratings, optical fibre, photoinduced stress, photoelasticity

1. Introduction

In the photoinscription process of Bragg grating (BG) in photosensitive Ge-doped SiO_2 glass without H_2 treatment, it is now accepted that a modification of the glass structure occurs which leads to specific volume change of the glass (glass densification) [1–4]. An earlier analytical model dealing with the stress distribution induced by the densification process was developed by Poumellec *et al* [5]. This model was a simplified approach of the physical phenomenon but sufficient enough to produce an approximated amplitude of the stress change, of the refractive index change and of the birefringence induced by BG writing, either in a preform slice (cubic symmetry) or in an optical fibre (cylindrical symmetry). Here, we describe a precise numerical approach of stress field generated by BG writing, which leads to a better spatial resolution of the stress change and refractive index change distributions. In addition, a new important result is the calculation of the shear component of stress tensor and the corresponding refractive index changes, in contrast with the first approach [5] or with other publications [6].

[1] Corresponding author. Tel: 0033169156351; fax: 0033169154797.

2. Theoretical background

2.1. Assumptions and approximations

(*a*) We consider a fibre containing a Bragg grating which is fabricated by UV irradiation of the fibre core using a suitable interferometric set-up [7–10]. The fibre is a cylinder of radius R_f containing an inner cylinder of radius R_c representing the fibre core. Consequently, it is better to use the cylindrical coordinates system (r, θ, z) for the representation of the problem (figure 1). The fibre is axisymmetric. Therefore, the components of the displacement field and the strain and stress tensors are not dependent on θ. The component of the displacement following θ, (u_θ) is zero, and the components of strain and stress following θ are also zero, i.e. $\varepsilon_{r\theta} = \varepsilon_{\theta r} = 0$ and $\sigma_{r\theta} = \sigma_{\theta r} = 0$. The displacement field, the strain and stress tensors are therefore

$$\vec{u}(r, z) = u_r(r, z)\vec{e}_r + u_z(r, z)\vec{e}_z \tag{1}$$

$$\bar{\bar{\varepsilon}} = \begin{pmatrix} \varepsilon_{rr} & 0 & \varepsilon_{rz} \\ 0 & \varepsilon_{\theta\theta} & 0 \\ \varepsilon_{rz} & 0 & \varepsilon_{zz} \end{pmatrix} \tag{2}$$

1464-4258/01/060429+11$30.00

$$\overline{\overline{\sigma}} = \begin{pmatrix} \sigma_{rr} & 0 & \varepsilon_{rz} \\ 0 & \sigma_{\theta\theta} & 0 \\ \sigma_{rz} & 0 & \sigma_{zz} \end{pmatrix}. \tag{3}$$

(*b*) At any point of the fibre, the Young modulus E and the Poisson ratio ν are assumed constant, and equal to those in pure silica ($E = 78$ GPa and $\nu = 0.162$) because the main part of the body, from the mechanical point of view, is pure silica.

(*c*) We assume that the fibre is exposed to an axisymmetric UV interference pattern and periodic along the fibre axis. Therefore, the distribution of UV light has no dependency on θ, and is expressed as

$$I(r, z) = 2I_0 \cos^2(\pi z/\Lambda) f(r) \tag{4}$$

where Λ is the grating period, I_0 is the mean UV power density (W cm^{-2}) and $f(r)$ is the radial UV intensity distribution normalized to unity. The visibility is thus assumed perfect.

(*d*) The UV photosensitivity profile of the glass (normalized to unity) is called $P(r)$ in the text below. The UV irradiation after absorption induces a local densification of the glass, i.e. a permanent strain distribution, which is assumed isotropic and proportional to the UV intensity and the photosensitivity profile. We get the following densification distribution:

$$\overline{\overline{\varepsilon^P}}(r, z) = \alpha . I(r, z) . P(r) . t . \overline{\overline{1}} \tag{5}$$

where t is the irradiation duration, α is a proportion coefficient fixed from experiment, and $\overline{\overline{1}}$ is the unit tensor. The total strain at each point of the body is made up of two parts. The first one is the permanent strain which is the local effect resulting from the photoinduced densification $\overline{\overline{\varepsilon^P}}$. The second part is the elastic strain $\overline{\overline{\varepsilon^e}}$ required to maintain the continuity of the body. The total strain is thus $\overline{\overline{\varepsilon}} = \overline{\overline{\varepsilon^e}} + \overline{\overline{\varepsilon^P}}$. The basic problem is the numerical evaluation of the elastic tensor $\overline{\overline{\varepsilon^e}}$ (output) according to the given permanent strain tensor (input) $\overline{\overline{\varepsilon^P}}$ under constraints, which are boundary conditions.

2.2. The equilibrium equations

The equilibrium equation in its vector form is

$$\text{div } \overline{\overline{\sigma}} = \vec{0} \tag{6}$$

where $\overline{\overline{\sigma}}$ is the stress tensor. As expressed in relation (3), the equilibrium equation (6), in the cylindrical coordinates system (r, θ, z), reduces to a couple of partial differential equations.

$$\begin{aligned} &\frac{\partial \sigma_{rr}}{\partial r} + \frac{\partial \sigma_{rz}}{\partial z} + \frac{\sigma_{rr} - \sigma_{\theta\theta}}{r} = 0 \\ &\frac{\partial \sigma_{rz}}{\partial r} + \frac{\partial \sigma_{zz}}{\partial z} + \frac{\sigma_{rz}}{r} = 0. \end{aligned} \tag{7}$$

Stress is related to strain in the following elasticity relation:

$$\overline{\overline{\sigma}} = \lambda \text{Tr}(\overline{\overline{\varepsilon}}) \overline{\overline{1}} + 2\mu \overline{\overline{\varepsilon}} - (3\lambda + 2\mu) \overline{\overline{\varepsilon^P}} \tag{8}$$

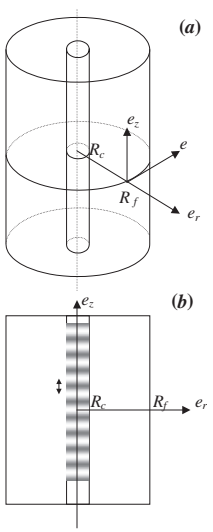

Figure 1. Optical fibre structure in the cylindrical coordinates system: (*a*) Three-dimensional scheme of the fibre showing the inner cylinder representing the core region of radius R_c and the outer cylinder of radius R_f. (*b*) Two-dimensional scheme of the longitudinal fibre section containing a Bragg grating of pitch Λ.

where $\overline{\overline{1}}$ is the unit tensor, Tr(ε) is the trace of the tensor ε. The Lamé elastic constant λ and μ are related to the Young modulus (E) and Poisson ratio (ν) as follows

$$\mu = \frac{E}{2(1+\nu)} \quad \text{and} \quad \lambda = \frac{E\nu}{(1+\nu)(1-2\nu)}. \tag{9}$$

Then the pertinent strain-displacement relations in the cylindrical coordinates system are given by

$$\begin{aligned} &\varepsilon_{rr} = \frac{\partial u_r}{\partial r}, \qquad \varepsilon_{\theta\theta} = \frac{u_r}{r}, \qquad \varepsilon_{zz} = \frac{\partial u_z}{\partial z} \\ &\varepsilon_{rz} = \frac{1}{2}\left(\frac{\partial u_r}{\partial z} + \frac{\partial u_z}{\partial r}\right) \\ &\varepsilon_{r\theta} = \varepsilon_{\theta z} = 0. \end{aligned} \tag{10}$$

The stresses are thus expressed in terms of displacements by relation (11):

$$\begin{aligned} \sigma_{rr} &= \lambda\left(\frac{\partial u_r}{\partial r} + \frac{u_r}{r} + \frac{\partial u_z}{\partial z}\right) + 2\mu\frac{\partial u_r}{\partial r} - (3\lambda + 2\mu)\varepsilon^p \\ \sigma_{\theta\theta} &= \lambda\left(\frac{\partial u_r}{\partial r} + \frac{u_r}{r} + \frac{\partial u_z}{\partial z}\right) + 2\mu\frac{u_r}{r} - (3\lambda + 2\mu)\varepsilon^p \\ \sigma_{zz} &= \lambda\left(\frac{\partial u_r}{\partial r} + \frac{u_r}{r} + \frac{\partial u_z}{\partial z}\right) + 2\mu\frac{\partial u_z}{\partial z} - (3\lambda + 2\mu)\varepsilon^p \\ \sigma_{rz} &= \mu\left(\frac{\partial u_r}{\partial z} + \frac{\partial u_z}{\partial r}\right). \end{aligned} \tag{11}$$

and finally the equilibrium equations in terms of displacements are

$$\begin{aligned} &(\lambda + 2\mu)\left(\frac{\partial^2 u_r}{\partial r^2} + \frac{1}{r}\frac{\partial u_r}{\partial r} - \frac{u_r}{r^2}\right) + \mu\frac{\partial^2 u_r}{\partial z^2} + (\lambda + \mu)\frac{\partial^2 u_z}{\partial z \partial r} \\ &\quad = (3\lambda + 2\mu)\frac{\partial \varepsilon^p}{\partial r} \\ &\mu\left(\frac{\partial^2 u_z}{\partial r^2} + \frac{1}{r}\frac{\partial u_z}{\partial r}\right) + (\lambda + 2\mu)\frac{\partial^2 u_z}{\partial z^2} \end{aligned}$$

$$+(\lambda+\mu)\left(\frac{\partial^2 u_r}{\partial z \partial r}+\frac{1}{r}\frac{\partial u_r}{\partial z}\right) = (3\lambda+2\mu)\frac{\partial \varepsilon^p}{\partial z}. \quad (12)$$

2.3. Boundary conditions

The equilibrium equation is solved by using the displacement method taking into account the following boundary conditions:

(*a*) The densification occurs mainly in the fibre core whose radius is very small compared to the fibre radius. We can consider, therefore that the radial displacement is zero at the fibre-free surface

$$u_r(R_{f,z}) = 0 \quad \text{for every} \quad z. \quad (13)$$

(*b*) According to the assumption of axisymmetry, the radial displacement is zero at the fibre axis

$$u_r(0, z) = 0 \quad \text{for every} \quad z. \quad (14)$$

(*c*) The grating length is assumed to be constant because the densification occurring in the irradiated fringes is compensated by an elastic dilatation in the dark fringes. Consequently, the axial displacement is zero at the centre of the bright and dark fringes where the densification is maximum and minimum, respectively

$$u_z(r, n.z/2\Lambda) = 0 \quad \text{for} \quad n \in Z \quad \text{and} \quad \forall r. \quad (15)$$

2.4. Numerical resolution of the problem

According to the assumptions of cylindricity, axisymmetry and periodicity the resolution domain is a longitudinal section of a half fibre.

$\Omega = 0 \leqslant r \leqslant R_f$ and
$0 \leqslant z \leqslant n\Lambda$ where n is an integer.

The finite element method has been used to solve the partial differential equation system (12). Both the mesh generation and the numerical resolution were achieved with the help of the FreeFEM software [11].

2.5. Photoinduced refractive index change

To calculate the refractive index change, it is better to use the Cartesian coordinate system (x, y, z) because the electric field during light propagation stands almost in the fibre section. The propagation indexes in the presence of the photoelastic effect are built up from the following contributions:

(i) The relative volume change $\frac{\Delta v}{v}$, i.e. the densification which is assumed isotropic using the Lorentz–Lorenz relation:

$$\Delta n_{ij}^{v} = -\frac{(n^2-1)(n^2+2)}{6n}\frac{\Delta v}{v} \quad \text{with} \quad \frac{(n^2-1)(n^2+2)}{6n} = 0.59 \quad \text{and} \quad \frac{\Delta v}{v} = \mathrm{Tr}(\overline{\overline{\varepsilon^P}}) = 3\varepsilon^P. \quad (16)$$

(ii) The photoelastic effect which is anisotropic. The elastic strain field $\overline{\overline{\varepsilon^e}}$ induces a change in the inverse of permittivity tensor $\Delta\overline{\overline{\eta}}$ via the following relation

$$\eta_{ij}\left(\varepsilon_{ij}^e - \eta_{ij}(0) = \Delta(1/n^2)\right)_{ij} = \sum_{k,l} p_{ijkl}\varepsilon_{kl}^e. \quad (17)$$

In (17), p_{ijkl} correspond to the photoelastic coefficients.

If we assume that the refractive index before UV irradiation n_0 was isotropic, the refractive index change can be written as

$$\Delta n_{ij}^e = -(n_0^3/2)\sum_{k,l} p_{ijkl}\varepsilon_{kl}^e. \quad (18)$$

Due to the symmetry of the elastic and photoelastic tensors, $p_{ijkl} = p_{jikl} = p_{ijlk}$ and $\varepsilon_{ij}^e = \varepsilon_{ji}^e$, the subscripts $ijkl$ can be contracted to mn, where m and n take the values from 1 to 6 (1, 2, 3, 4, 5, 6 for xx, yy, zz, yz, xz, xy), one can write $p_{ijkl} = p_{jikl} = p_{ijlk} = p_{mn}$ and $\varepsilon_{ij}^e = \varepsilon_{ji}^e = \varepsilon_n^e$. We get:

$$\Delta n_m^e = -(n_0^3/2)\sum_{k,l} p_{mn}\varepsilon_n^e. \quad (19)$$

For an isotropic body, the expression of the photoelastic tensor $\overline{\overline{p}}$, in a Cartesian coordinate (x, y, z), is given by

$$\overline{\overline{p}} = \begin{pmatrix} p_{11} & p_{12} & p_{12} & 0 & 0 & 0 \\ p_{12} & p_{11} & p_{12} & 0 & 0 & 0 \\ p_{12} & p_{12} & p_{11} & 0 & 0 & 0 \\ 0 & 0 & 0 & \frac{1}{2}(p_{11}-p_{12}) & 0 & 0 \\ 0 & 0 & 0 & 0 & \frac{1}{2}(p_{11}-p_{12}) & 0 \\ 0 & 0 & 0 & 0 & 0 & \frac{1}{2}(p_{11}-p_{12}) \end{pmatrix}. \quad (20)$$

In contrast, the strain tensor $\overline{\overline{\varepsilon^e}}$ is known only in a cylindrical coordinate (r, θ, z)

$$\overline{\overline{\varepsilon}} = \begin{pmatrix} \varepsilon_{rr}^e & 0 & \varepsilon_{rz}^e \\ 0 & \varepsilon_{\theta\theta}^e & 0 \\ \varepsilon_{rz}^e & 0 & \varepsilon_{zz}^e \end{pmatrix}. \quad (21)$$

We need to express $\overline{\overline{\varepsilon^e}}$ in the Cartesian coordinate (x, y, z). For that purpose, we use the conversion matrix from Cartesian to cylindrical coordinates defined by

$$\overline{\overline{a}} = \begin{pmatrix} \cos\theta & \sin\theta & 0 \\ -\sin\theta & \cos\theta & 0 \\ 0 & 0 & 1 \end{pmatrix}. \quad (22)$$

We obtain the following expression of $\overline{\overline{\varepsilon^e}}$ in the system (x, y, z)

$$\varepsilon_{ij}^{e'} = a_{li}a_{kj}\varepsilon_{ij}^e = \begin{pmatrix} \cos^2\theta\varepsilon_{rr}^e + \sin^2\theta\varepsilon_{\theta\theta}^e & -\sin\theta\cos\theta \times(\varepsilon_{rr}^e - \varepsilon_{\theta\theta}^e) & \cos\theta\varepsilon_{rz}^e \\ -\sin\theta\cos\theta \times(\varepsilon_{rr}^e - \varepsilon_{\theta\theta}^e) & \sin^2\theta\varepsilon_{rr}^e + \cos^2\theta\varepsilon_{\theta\theta}^e & -\sin\theta\varepsilon_{rz}^e \\ \cos\theta\varepsilon_{rz}^e & -\sin\theta\varepsilon_{rz}^e & \varepsilon_{zz}^e \end{pmatrix}. \quad (23)$$

If we use the contracted subscripts, the components of the strain tensor in the Cartesian coordinates will be the following:

$$\begin{aligned}
\varepsilon_1^{e'} &= \cos^2\theta\varepsilon_{rr}^e + \sin^2\theta\varepsilon_{\theta\theta}^e \\
\varepsilon_2^{e'} &= \sin^2\theta\varepsilon_{rr}^e + \cos^2\theta\varepsilon_{\theta\theta}^e \\
\varepsilon_3^{e'} &= \varepsilon_{zz}^e \\
\varepsilon_4^{e'} &= -\sin\theta\varepsilon_{rz}^e \\
\varepsilon_5^{e'} &= \cos\theta\varepsilon_{rz}^e \\
\varepsilon_6^{e'} &= \cos\theta\sin\theta(\varepsilon_{\theta\theta}^e - \varepsilon_{rr}^e).
\end{aligned} \tag{24}$$

The tensor of photoelastic refractive index change in the Cartesian coordinate can be obtained using the relations (20), (21) and (24):

$$\begin{aligned}
\Delta n_{xx}^e &= -\frac{n_0^3}{2}\Big[p_{11}\left(\cos^2\theta\varepsilon_{rr}^e + \sin^2\theta\varepsilon_{\theta\theta}^e\right) \\
&\quad + p_{12}\left(\sin^2\theta\varepsilon_{rr}^e + \cos^2\theta\varepsilon_{\theta\theta}^e + \varepsilon_{zz}^e\right)\Big] \\
\Delta n_{yy}^e &= -\frac{n_0^3}{2}\Big[p_{11}\left(\sin^2\theta\varepsilon_{rr}^e + \cos^2\theta\varepsilon_{\theta\theta}^e\right) \\
&\quad + p_{12}\left(\cos^2\theta\varepsilon_{rr}^e + \sin^2\theta\varepsilon_{\theta\theta}^e + \varepsilon_{zz}^e\right)\Big] \\
\Delta n_{zz}^e &= -\frac{n_0^3}{2}\left[p_{11}\varepsilon_{zz}^e + p_{12}\left(\varepsilon_{rr}^e + \varepsilon_{\theta\theta}^e\right)\right] \\
\Delta n_{xy}^e &= -\frac{n_0^3}{2}\left[\frac{1}{2}(p_{11} - p_{12})\sin\theta\cos\theta\left(\varepsilon_{\theta\theta}^e - \varepsilon_{rr}^e\right)\right] \\
\Delta n_{xz}^e &= -\frac{n_0^3}{2}\left[\frac{1}{2}(p_{11} - p_{12})\cos\theta\varepsilon_{rz}^e\right] \\
\Delta n_{yz}^e &= -\frac{n_0^3}{2}\left[-\frac{1}{2}(p_{11} - p_{12})\sin\theta\varepsilon_{rz}^e\right].
\end{aligned} \tag{25}$$

Δn has a cylindrical symmetry, therefore we can think on $\theta = 0$ (polarization parallel to x), the relations (25) become

$$\begin{aligned}
\Delta n_{xx}^e &= -\frac{n_0^3}{2}\left[p_{11}\varepsilon_{rr}^e + p_{12}\left(\varepsilon_{\theta\theta}^e + \varepsilon_{zz}^e\right)\right] \\
\Delta n_{yy}^e &= -\frac{n_0^3}{2}\left[p_{11}\varepsilon_{\theta\theta}^e + p_{12}\left(\varepsilon_{rr}^e + \varepsilon_{zz}^e\right)\right] \\
\Delta n_{zz}^e &= -\frac{n_0^3}{2}\left[p_{11}\varepsilon_{zz}^e + p_{12}\left(\varepsilon_{rr}^e + \varepsilon_{\theta\theta}^e\right)\right] \\
\Delta n_{xy}^e &= 0, \quad \Delta n_{xz}^e = -\frac{n_0^3}{2}\left[\frac{1}{2}(p_{11} - p_{12})\varepsilon_{rz}^e\right], \quad \Delta n_{yz}^e = 0.
\end{aligned} \tag{26}$$

Then, the total refractive index change tensor is the sum of contribution from the volume change Δn^v (16) and from the photoelastic one Δn^e (13). We get:

$$\begin{aligned}
\Delta n_{xx} &= -\frac{n_0^3}{2}\left[p_{11}\varepsilon_{rr}^e + p_{12}\left(\varepsilon_{\theta\theta}^e + \varepsilon_{zz}^e\right)\right] + \frac{(n^2-1)(n^2+2)}{2n}\varepsilon^P \\
\Delta n_{yy} &= -\frac{n_0^3}{2}\left[p_{11}\varepsilon_{\theta\theta}^e + p_{12}\left(\varepsilon_{rr}^e + \varepsilon_{zz}^e\right)\right] + \frac{(n^2-1)(n^2+2)}{2n}\varepsilon^P \\
\Delta n_{zz} &= -\frac{n_0^3}{2}\left[p_{11}\varepsilon_{zz}^e + p_{12}\left(\varepsilon_{rr}^e + \varepsilon_{\theta\theta}^e\right)\right] + \frac{(n^2-1)(n^2+2)}{2n}\varepsilon^P \\
\Delta n_{xy} &= 0, \quad \Delta n_{xz} = -\frac{n_0^3}{2}\left[\frac{1}{2}(p_{11} - p_{12})\varepsilon_{rz}^e\right], \quad \Delta n_{yz} = 0.
\end{aligned} \tag{27}$$

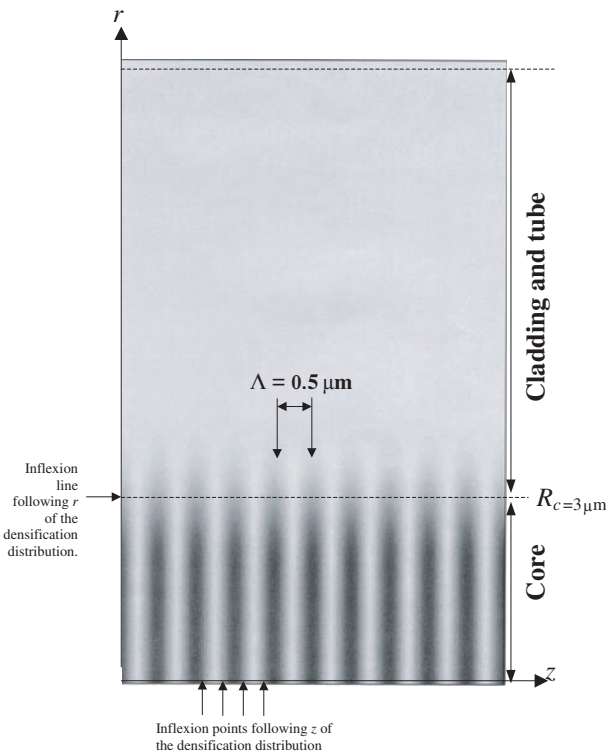

Figure 2. Densification distribution represented by the isotropic permanent strain $\varepsilon^P(r, z)$ in the fibre section used as an input data for the stress calculation. The picture is coded in grey scale: the dark regions are for bright fringes. The two black arrows indicate two irradiated fringes, the distance between them (the grating period, Λ is 0.5 μm. The permanent strain, (i.e. 1/3 of the specific volume change) $\varepsilon^P(r, z)$ is negative. Its radial profile passing at the centre of an irradiated fringe has been chosen Gaussian (the minimum value is -3×10^{-3}, the white is for zero). Inflexion points following z or r are in the middle of the fringes or at the core-cladding interface.

3. Results and discussion

3.1. Example of solution

In the example below, we consider a fibre of $R_f = 62.5$ μm external radius, and a core of 3 μm radius containing a grating with $\Lambda = 0.5$ μm pitch. The densification distribution $\varepsilon^P(r, z)$ which is the main input data of the problem (relation (5)), is periodic following the fibre axis and is assumed to have a Gaussian radial profile (maximum at the core centre and decreases rapidly to zero at the fibre-free surface). Its maximum absolute value at the core centre is about 3×10^{-3}. This value was obtained from the measurement of the topography surface of an optical fibre preform irradiated with ordinary Bragg grating elaboration conditions (a few kJ cm^{-2} [5]). As shown in figure 2, ε^P is negative because the permanent strain induced by UV irradiation is a compaction process according to the observation made by B Poumellec *et al* [1] and P Cordier *et al* [3].

3.1.1. Displacements. Figures 3 and 4 show the radial and axial displacements resulting from the densification distribution ε_p, displayed in figure 2. The radial displacement is negative and has a weak modulation along the grating axis as can be noted in figure 3(a). The radial profile of

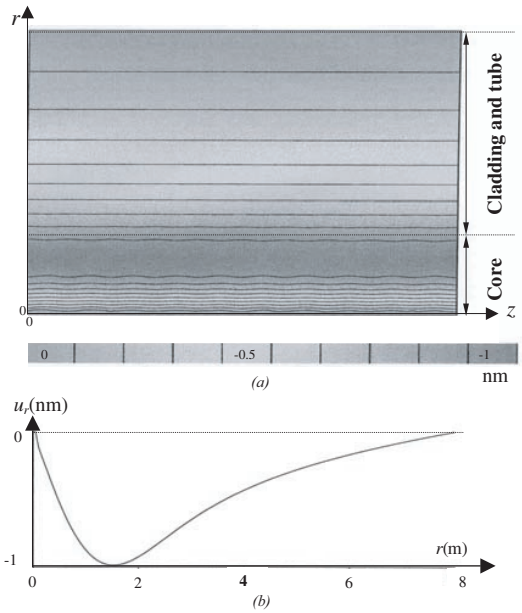

Figure 3. (*a*) Radial displacement distribution in the fibre section. (*b*) Radial profile at $z = 0$.

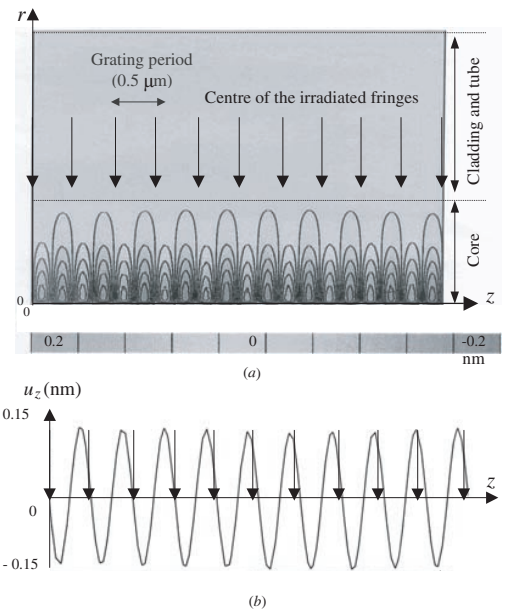

Figure 4. (*a*) Axial displacement distribution in the fibre section. (*b*) Axial profile at $r = R_c/4$.

$u_r(r, z)$ on a fringe ($z = 0$) is shown in figure 3(*b*). The minimum of $u_r(r, z)$ is located inside the core close to the core-cladding boundary. Its value, for the example considered here, is about -1 nm. The physical interpretation of the results is that the matter moves everywhere towards the fibre axis due to compaction (radial shrinkage). Figure 4 shows the axial displacement $u_z(r, z)$which is, in contrast with the radial displacement, strongly modulated along the grating axis. The amplitude of the peak-to-peak modulation is about 0.3 nm (see figure 4(*b*)). It is maximum and minimum, alternatively, along the grating axis, at the points corresponding to $z = (2n + 1)\Lambda/4$, with n being the integer i.e., the inflexion points of the densification distribution (figure 2). Consequently, the non-irradiated fringes are dilated whereas the irradiated fringes are contracted.

3.1.2. Stress field. Using the above displacements, the stress field is calculated by means of the stress-strain (12) and strain-displacement relations (11). The four non-zero components of the stress tensor ($rr, \theta\theta, zz$ and rz) are shown in figure 5. We notice that the stress components calculated here are the components of the stress induced by the densification, in addition to the residual stress due to heterogeneity of the optical fibre. Therefore, σ_{ij} will be conveniently noted $\Delta\sigma_{ij}$. The perpendicular components $\Delta\sigma_{rr}$ and $\Delta\sigma_{\theta\theta}$ are modulated along the grating axis. The minimum is -70 MPa at the centre of the non-irradiated fringes and the maximum is 236 MPa at the centre of the irradiated fringes. The mean value of $\Delta\sigma_{rr}$ is about 195 MPa. The behaviour of the two components $\Delta\sigma_{rr}$ and $\Delta\sigma_{\theta\theta}$ are quite similar all over the fibre section. The difference between them, i.e., $\Delta\sigma_{rr} - \Delta\sigma_{\theta\theta}$, is represented in figure 6, showing that the largest value is localized at the core-cladding interface. We can also observe in figure 5 that $\Delta\sigma_{rr}$ and $\Delta\sigma_{\theta\theta}$ decrease rapidly in the radial direction from the core centre to the fibre outside. In contrast, the axial component $\Delta\sigma_{zz}$ exhibits a weak modulation along the grating axis (130 MPa (for non-irradiated fringes), 195 MPa (for irradiated fringes)) and decreases slowly in the radial direction from the grating axis to the fibre outside. The shear stress component $\Delta\sigma_{rz}$ (see figure 5) is small relative to the diagonal components (10%). Its modulation ranges between -13 MPa and +13 MPa. The peak of the modulations are localized at the points corresponding to $z = (2n + 1)/\Lambda$, where n is an integer i.e., between the bright and dark fringes.

At $z = n\Lambda/2$, i.e., the centre of the irradiated and non-irradiated regions, the shear stress is zero.

3.1.3. Photoinduced index change. Figure 7 shows the refractive index change tensor components xx, yy, zz, xz according to relation (28). The shear component Δn_{xz} is purely photoelastic because it is a non-diagonal component of the refractive index tensor. It is alternate along the grating axis and its amplitude, for the example considered here, is small ($\Delta n_{xz}^{\text{mod}} = 9 \times 10^{-5}$) compared to the diagonal components. We have seen that it increases with the grating period contrary to the three other components xx, yy, zz. The diagonal components $\Delta n_{xx}\Delta n_{yy}\Delta n_{zz}$ results of two contributions: the photoelastic contribution which is 40% of the contribution due to volume change. This explains why the modulation on the axial component of the refractive index change tensor Δn_{zz} (see figure 7) are more contrasted than the one of the axial stress component $\Delta\sigma_{zz}$ (see figure 5). In contrast, the modulation of Δn_{zz} is smaller than the modulation for the perpendicular components Δn_{xx} and Δn_{yy}. Their values for a polarization along the x axis are

$$\Delta n_{xx}^{\text{mod}} = 1.710^{-4},\ \Delta n_{yy}^{\text{mod}} = 1.810^{-4} \text{ and } \Delta n_{zz}^{\text{mod}} = 1.410^{-4}.$$

$$[\Delta n_{xx}] = 1.810^{-4},\ [\Delta n_{yy}] = 1.910^{-4} \text{ and } [\Delta n_{zz}] = 1.910^{-4}.$$

It is interesting to note that even if the visibility of the UV interference pattern is perfect, the mean index change is larger than the amplitude of the modulation and this is due to the non-local action of the elastic field.

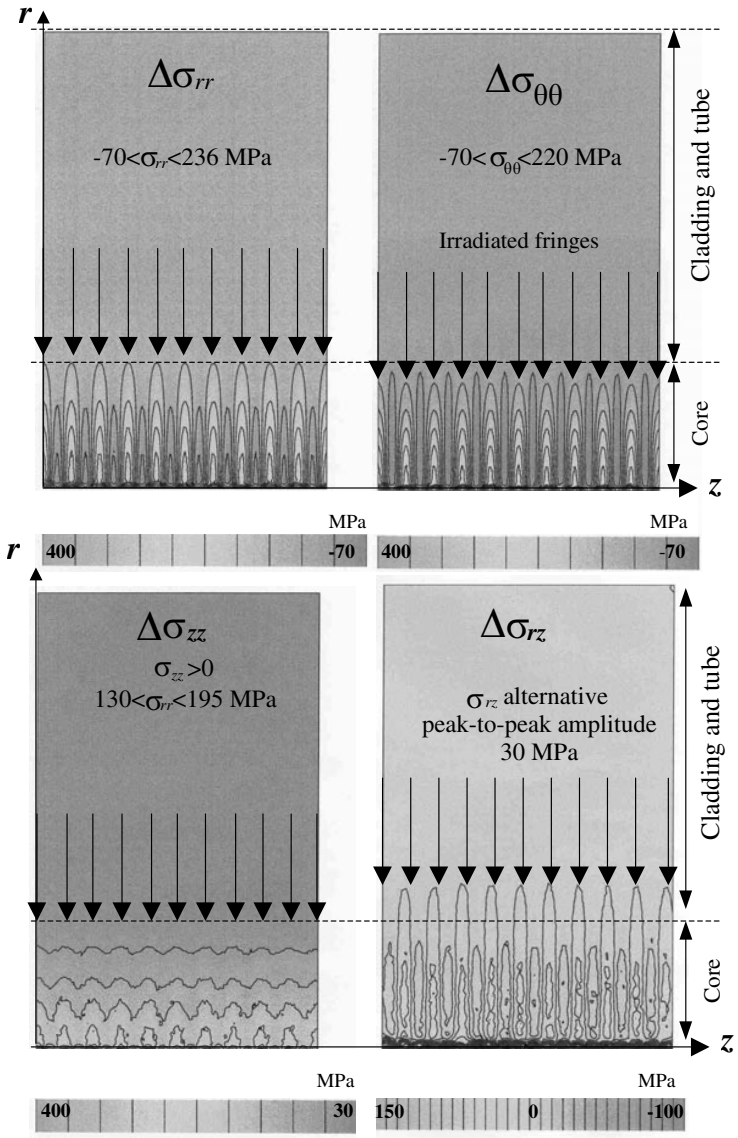

Figure 5. The three diagonal ($rr, \theta\theta, zz$) and the shear (rz) components of the stress tensor in MPa. The black arrows along the grating indicate the centre of the bright fringes.

The values above the modulation and mean index change can be written in terms of permanent strain because of the linearity : $\Delta n_{\perp}^{\mathrm{mod}} = 0.57\varepsilon^P$ and $[\Delta n_{\perp}] = 0.60\varepsilon^P$, these two quantities are closer than those in the analytical model of Poumellec *et al* [5] because here the average value of perpendicular deformation ε_{rr} is positive due to cladding resistance whereas it was assumed zero in the analytical model. For the same reason, the fibre axis elastic deformation ε_{zz}^e is here modulated in phase with ε^p, whereas it was flat in the analytical model [5].

3.2. Shear stress at the core-cladding interface

Taking the particular case of a step profile for the radial densification distribution (see figure 8), i.e., a maximum densification in the fibre core and no densification outside the core, the behaviour of the stress diagonal components are in agreement with the analytical model [5]. In this case, the shear stress (see figure 8(a)) are distributed at the core-cladding interface. $\Delta\sigma_{rz}$ is zero all over the fibre except at the core-cladding interface, where it is periodic and alternating along the grating axis. The axial profile of the shear stress at $r = R_c$ is shown in figure 8(c) for the following case: a fibre of 62.5 μm radius, a core radius $R_c = 3$ μm, a grating period $\Lambda = 1\mu$m and a densification distribution with a maximum peak-to-peak value at the centre of the fibre core of 3.1×10^{-3}.

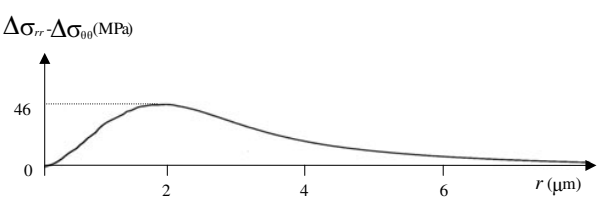

Figure 6. Radial profile of stress birefringence ($\sigma_{rr} - \sigma_{\theta\theta}$).

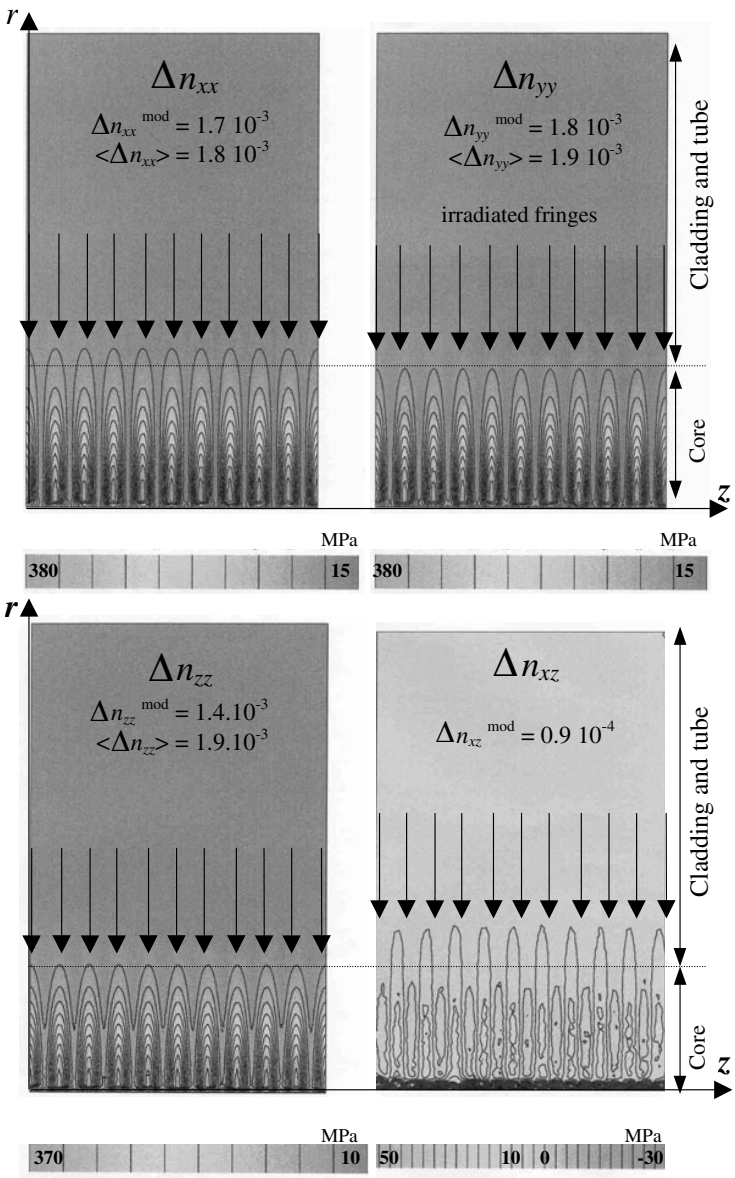

Figure 7. The three diagonal (xx, yy, zz) and the shear (xz) components of the refractive index change tensor in a Cartesian coordinate system ($\theta = 0$). The black arrows along the grating indicate the centre of the irradiated fringes.

The values of stresses for the four components rr, $\theta\theta$, zz and rz for several densification distribution and several values of the gratings period are summarized in table 1.

As pointed out previously, the shear components of strain, stress and refractive index change, in contrast with the other three diagonal components, increase on the grating period. It ranges between $[-24, 24]$ MPa for $\Lambda = 0.5\ \mu$m and between $[-122, 122]$ MPa for $\Lambda = 1\ \mu$m (see table 1) for a step densification profile. This is due to the increase of the axial displacement on grating period. We emphasize that shear stress modulation is large, in this case, compared to the value of diagonal stress in the core (122 compared to 150). On the other hand, to the shear stress, it corresponds to an off-diagonal refractive index component whose value, in the above case, ranges between -4×10^{-4} and 4×10^{-4} compared to peak-to-peak perpendicular refractive index modulation (4×10^{-3}).

3.3. Verification of the sum rule '$\sigma_{zz} = \sigma_{rr} + \sigma_{\theta\theta}$'

The set-up for the measurement of stress in fibres is described by Chu *et al* [13]. A He-Ne laser, linearly polarized at 45° to the fibre axis, is focused on the fibre transversally. The beam, the radial distribution of the axial stress, σ_{zz}, is obtained by measuring the optical retardation between the index components parallel and perpendicular to the fibre axis in moving the beam along a diameter. The radial and circumferential stress components σ_r and σ_θ are obtained from the axial component σ_z using the sum rule, i.e., $\sigma_{zz}(r) = \sigma_{rr}(r) + \sigma_{\theta\theta}(r)$ and the equilibrium equation (5). On the other hand, in a lot of other stress calculation problems in fibres, the sum rule is used, especially for the thermal stresses calculation. Figure 9 shows the distribution of $\sigma_{zz}(r) - [\sigma_{rr}(r) + \sigma_{\theta\theta}(r)]$ for the example considered in section 3.1. We can observe that the sum rule is correct in average on the grating length, but is

Table 1. Dependence of the stress components with the grating period for Gaussian and step densification radial profiles.

Densification profile Grating period (MPa)	Gaussian $\Lambda = 0.5\mu$m	Gaussian $\Lambda = 1\mu$m	Gaussian $\Lambda = 2.5\mu$m	Step $\Lambda = 0.5\mu$m	Step $\Lambda = 1\mu$m
$[\Delta\sigma_{zz}]$	165	165	165	152	152
$[\Delta\sigma_{rr}]$	154	154	154	150	150
$[\Delta\sigma_{\theta\theta}]$	152	152	152	150	150
$\Delta\sigma_{zz}^{\text{mod}}$	65	65	65	26	26
$\Delta\sigma_{rr}^{\text{mod}}$	310	310	310	316	316
$\Delta\sigma_{\theta\theta}^{\text{mod}}$	275	294	294	326	326
max $\Delta\sigma_{rz}^{\text{mod}}$	26	50	108	48	244

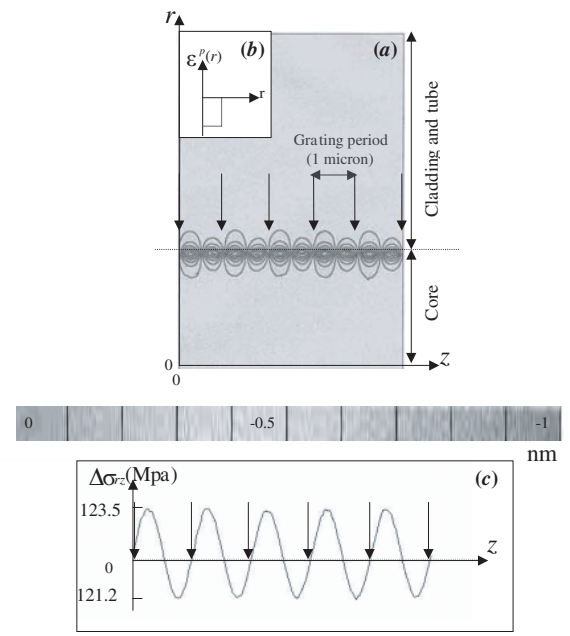

Figure 8. (a) Shear stress $\Delta\sigma_{rz}$ for a step densification profile shown in (b) and a grating period of 1 μm, (c) is the axial profile at the core-cladding interface, i.e., $\Delta\sigma_{rz}(r = R_c)$. The black arrows along the grating in (a) and the black arrows in (c) indicate the centre of the irradiated fringes.

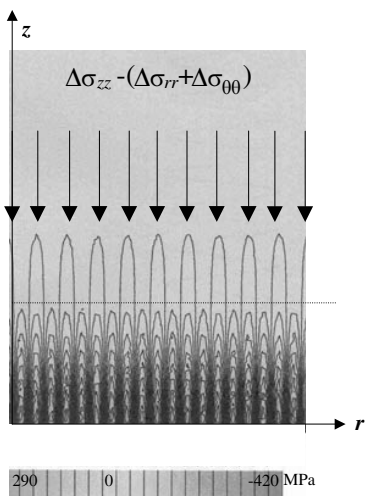

Figure 9. Test of the sum rule $\sigma_{zz} = \sigma_{rr} + \sigma_{\theta\theta}$ in a fibre section containing a Bragg grating.

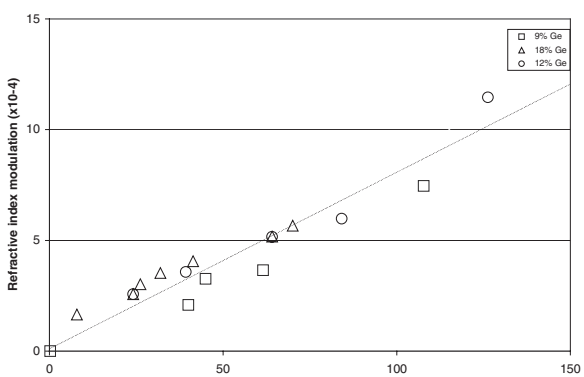

Figure 10. Relationship between refractive index modulation and the mean axial stress change for three different fibres (after [15]).

not valid between the grating fringes. The calculation of the components σ_{rr} and $\sigma_{\theta\theta}$ will not be correct using the sum rule in the case of a grating whose period is larger than the He-Ne laser diameter used to measure the stresses [14]. But, a He-Ne spot diameter of 3 μm and a grating of 0.5 μm pitch leads to an averaging along six grating fringes and the sum rule is valid.

3.4. Comparison with the measurements

Here, we compare our calculations with the measurements of Fonjallaz *et al* [15]. Figure 10 shows refractive index modulation versus mean axial stress change, for three Ge-doped fibres (9, 12 and 18 in mol%) and containing a Bragg grating written with 31 kJ cm^{-2}, 31 kJ cm^{-2} and 15 kJ cm^{-2}, respectively. The relation between the index modulation of the perpendicular index $\Delta n_{\perp}^{\text{mod}}$ and the mean axial stress component $[\Delta\sigma_{zz}]$ is linear and the slope is estimated experimentally to $(0.8\pm0.2)10^{-11}$ Pa^{-1} [15]. $\Delta n_{\perp}^{\text{mod}}$ and $[\Delta\sigma_{zz}]$, calculated in the example of section 3.1, are respectively, 1.7×10^{-3} and 165 MPa, thus the calculated slope is 1.03×10^{-11} Pa^{-1}, which is in good agreement with the measured one.

3.5. Comparison with the analytical model of Poumellec et al [5]

In the analytical model reported by Poumellec *et al* [5], the slope $\frac{\Delta n_{\text{mod}}}{\langle\sigma_z\rangle}$ is about 1.2×10^{-11} Pa^{-1}, and has the following analytical expression

$$\Delta n_{\perp}^{\text{mod}} = \left[-\frac{n^3}{4}\left(p_{11} + p_{12}\right) + \frac{\left(n^2-1\right)\left(n^2+2\right)}{4n} \right] \frac{\langle\sigma_z\rangle}{\frac{\lambda}{2}+\mu}.$$

The value of the slope is larger than the value obtained by the finite element model (FEM). This difference is due to the perpendicular mechanical reaction of the cladding and tube which is taken into account properly in FEM. It is worth noting that, for the analytical model, the relation between the mean axial stress and the maximum (in absolute value) of the permanent strain (densification) is given by the relation $\langle\sigma_z\rangle = \frac{\lambda+2\mu}{2}\varepsilon^P_{\max}$. Therefore, using data of section 3.1, we get $\langle\sigma_z\rangle = 135$ MPa. For the FEM model the corresponding value is about 165 MPa. We have also compared the strain tensors for both FEM using an analytical model, the main points arising from the comparison are the following:

- For both models we have: $[\varepsilon^e_{zz}] = -\varepsilon^P_{zz}/2$
- For FEM ε^e_{zz} is modulated between 1.3×10^{-3} to 1.8×10^{-3} in phase with ε^P_{zz}, whereas it was flat in the analytical model. The modulation is due to the non-diagonal effect of the cladding resistance. Therefore, ε^T_{zz} exhibits a larger modulation than the one of ε^P_{zz}.
- $\varepsilon^{e\,\mathrm{mod}}_{\perp}$ is out of phase with $\varepsilon^P_{\perp}$ as in the analytical model. However, the $[\varepsilon^e_{\perp}]$ is not negligible and is positive. This is due to the mean cladding resistance, which is taken into account here.

3.6. Birefringence calculations

3.6.1. Interpretation of the grating birefringence observed in the preform plate. For computing the birefringence for a free propagation parallel to the $\vec{y}$ axis and transversal to the grating axis $\vec{z}$, it is necessary to know the main propagation indexes n' and n'' in the wave plane xz. The perpendicular plane to the propagation direction cuts the index ellipsoid, of equation $\eta_{ij}x_ix_j = 1$, in an elliptical section in which the long and short axis define two indexes and two directions for the polarization projection. We have calculated these two main indexes n' and n'' from the diagonalization of the 2×2 matrix representing the minor xz of the refractive index change tensor (27). The birefringence is the difference between n' and n'', i.e.,

$$n' - n'' = \frac{n_0^3}{2}(p_{12} - p_{11})\left[(\varepsilon_{rr} - \varepsilon_{zz})^2 + (\varepsilon_{rz})^2\right]^{1/2}.$$

This quantity is proportional to $\left[(\sigma_{rr} - \sigma_{zz})^2 + (\sigma_{rz})^2\right]^{1/2}$ which is shown in figure 11(b). Therefore, this figure displays the birefringence distribution for free propagation transversal to grating axis. We can observe that it is mainly distributed on the non-irradiated fringes where its value is four times larger than in the irradiated fringes. Figure 11(a) shows a polarized-analysed optical microscope image of three parallel gratings (10 μm pitch) written in SiO_2-GeO_2 preform core which was previously and partially coated by a carbon layer. The irradiated fringes are delimited by the places where the carbon layer was evaporated by the UV beam. The central grating was written at a place not covered by the carbon layer (in the centre of figure 11(a)). We can observe on this grating (the central one) that the maximum of light (the white regions on the figure) are between irradiated fringes indicating that the maximum of birefringence are reached on the non-irradiated fringes as it is found in our calculations.

3.6.2. Birefringence for guided propagation in fibre. For the guided propagation, the electric induction field $\vec{D}$ is not perpendicular to the propagation direction. Therefore, the calculation of $\Delta\vec{E}$ or $\Delta\vec{D}$ is not as simple as for free propagation. However, $\vec{D}$ proceeds over the index ellipsoid (the same for the electric field $\vec{E}$ in free medium). In fact, $8\pi W_e = {}^t\vec{D}\bar{\bar{\varepsilon}}^{-1}\vec{D} = D^2/n^2$ (W_e is the electric power density and n is the index in the direction parallel to $\vec{D}$). In contrast, the wave plane containing $\vec{D}$ will become conic and the indexes will be defined from the intersection of this conic with the index ellipsoid, which is not so simple to get because the index equation of Fresnel is no longer valid. To study the birefringence of propagation, we have neglected the component following $\vec{z}$ and assumed that $\vec{D}$ is parallel to $\vec{x}$. Knowing that the propagation direction is parallel to the grating axis, and $\Delta n_{xy} = 0$ for $\theta = 0$, the change in main propagation indexes n' and n'' will correspond to Δn_{xx} and Δn_{yy} (the minor xy of the tensor of refractive index change (27) is diagonal). According to relation (27), we have

$$n' - n'' = \Delta n_{xx} - \Delta n_{yy} = -\frac{n_0^3}{2}(p_{11} - p_{12})(\varepsilon_{rr} - \varepsilon_{\theta\theta}).$$

This quantity is proportional to $\Delta\sigma_{rr} - \Delta\sigma_{\theta\theta}$ as shown in figure 6. We can observe that the birefringence is maximum at the core-cladding interface, i.e., the inflexion points of the density distribution. This non-homogeneous quantity in the fibre section can induce a modal polarization dispersion in the presence of a grating photoinduced ovality of the fibre core.

4. Consequences

We have shown that the shear stress σ_{rz} is growing with the grating pitch. The peaks of σ_{rz} modulation are localized at the inflexion points of the densification distribution. Therefore the long period gratings develop high shear stresses. These high stresses can be also developed, when the visibility is bad or for uniform irradiation and can be responsible of mechanical degradation of the glass, such as fracture growth. Figure 12(a) shows periodic cracks resulting from a uniform irradiation of Ge-doped preform cut following its axis. The core area of 15 mm $\times$ 0.5 mm has been irradiated with a uniform beam with a pulsed laser at 193 nm using 55 000 pulses at 350 mJ cm^{-2} and a repetition rate of 30 Hz at PhLAM Laboratory, Lille University. An enlargement of the framed region in the left-hand side of figure 12(a) is shown in figure 12(b). Figure 12(c) is a topography surface of the framed region at the centre of figure 12(a) showing several cracks which are indicated by white arrows (in white the level is at 190 nm and in black the level is at -147 nm). We observed a main depletion of the core surface corresponding to the densification process (the cladding is at zero level) and a surface upheaval at the cracks which is the result of the stress relaxation.

We have noticed that the slope of $\Delta n^{\mathrm{mod}}_{\perp}$ versus $[\Delta\sigma_{zz}]$ calculated with the analytical and finite element models (1.2 and 1.0 respectively) are quite a lot larger than 0.8 of the experimental slope (0.8). We have checked that this discrepancy is not due to the hypothesis considering the Young modulus E and the Poisson's ratio ν constant in the fibre section. Using a calculation in which the above hypothesis

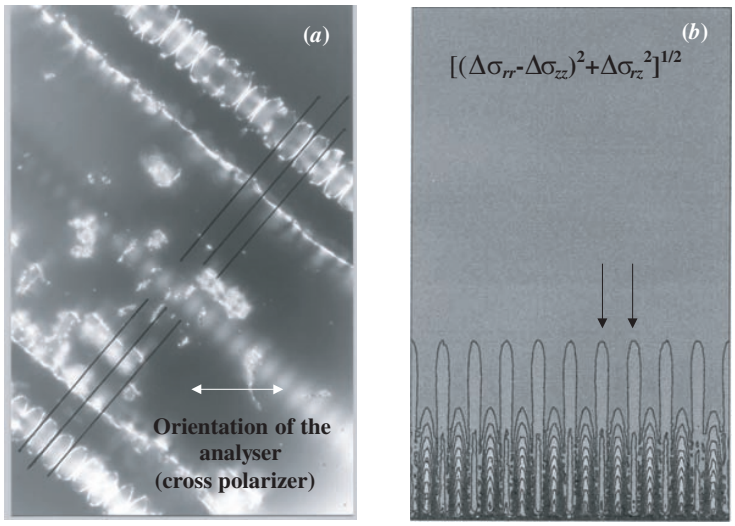

Figure 11. (*a*) Polarized-analysed optical microscope image of three parallel gratings (10 μm pitch) written in Ge-doped preform core previously coated partially by a carbon layer. The grating at the top right and at the bottom left were written through a carbon layer for tracking the bright fringes. The grating at the centre of the picture was written where no carbon layer was deposited. (*b*) Distribution of $\sqrt{(\sigma_{rr}-\sigma_{zz})^2+(\sigma_{rz})^2}$ which is proportional to the birefringence for free propagation transversal to the grating axis (65 MPa on irradiated fringe and 211 MPa on non-irradiated fringe). The grey scale is the same as in figure 9. The two black arrows indicate the centre of two irradiated fringes. The birefringence is maximum on the dark fringe.

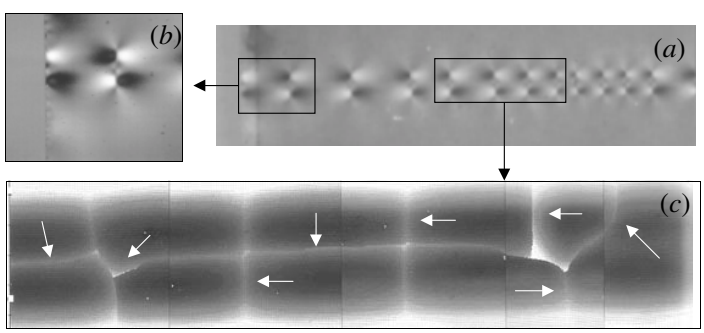

Figure 12. (*a*) Optical image of UV-induced cracks in the core of a preform (Ge-doped with 15 wt% SiO_2) cut following its axis. The core area of 15 mm $\times$ 0.5 mm has been irradiated with a uniform beam using a pulsed laser at 193 nm with 55 000 pulses at 350 mJ cm^{-2} and a repetition rate of 30 Hz at PhLAM Laboratory, University of Lille. (*b*) Enlargement of the framed region in the left-hand side of (*a*). (*c*) Surface topography of the framed region at the centre of (*a*) showing several cracks indicated by white arrows (in white the level is at 190 nm and in black the level is at -147 nm). The cladding is at the zero level far from the interface.

was relaxed, we have shown that even if E and ν reach a maximum variation of 20% in the fibre section the final result has less than 10% change. Other possible reasons are the chemical dependence of refractive index and photoelastic coefficients which were not taken into account. We have no information about photoelastic dependence with the chemical composition but we do know that for the refractive index, 13 mol% GeO_2 modifies the index by only 1% which is negligible for changing the value of the slope. Another possible reason is the photochromism contribution to total refractive index change. It is well known that after irradiation there is a change in absorption spectrum in the UV region [16–19] which is also depending of the stress [5] and according to Kramers–Kronig there is a contribution to refractive index change. The estimation of this contribution to the total refractive index modulation is at least 10%. All these reasons may be acting together to explain the 10% disagreement between the FEM calculated and measured slopes.

It is worth noting that Δn_{mod} and $[\Delta n]$ appear close in the calculation as it is observed in fibres without H_2 loading [20].

5. Conclusion

The stress field induced by Bragg grating inscription in fibre is calculated here using the finite element method and leads to a index modulation in the perpendicular direction of the propagation. The relation between the modulation of the perpendicular index $\Delta n_{\perp}^{\mathrm{mod}}$ and the mean axial stress change $[\Delta\sigma_{zz}]$ is linear and the slopes measured and calculated are in good agreement. The birefringence associated with the stress field has been evaluated. We have calculated the birefringence for a free propagation parallel to the $\vec{y}$ axis and transversal to the grating axis $\vec{z}$. We have shown, as was observed experimentally, that it is mainly distributed in the non-irradiated fringes than in the irradiated fringes. In addition, the birefringence of propagation is mainly located at the core-cladding interface, i.e., at the inflexion point of the densification distribution. This inhomogeneity in the fibre section can induce a modal polarization dispersion in the presence of a grating photoinduced ovality of the fibre core.

An important feature resulting from the numerical calculation of the stress field during Bragg grating inscription is the development of a shear stress component which can reach large values at the inflexion points of the densification distribution. Therefore, cracks at the core–cladding interface can be developed, leading to large scattering as observed by Janos *et al* [21]. It is worth noting that the type IIA [22] is recognized to occur at the core–cladding interface. In addition, σ_{rz} gives rise to n_{rz} which is likely to be at the origin of optical losses. As the shear stress increases on the spatial period, we can expect large shear stress between fringes, especially for long period gratings. On the other hand, when the mean index becomes larger than the index modulation (visibility less than 100%), the compensation between the bright and dark fringes is not achieved within a period and stress is accumulated along the grating leading to cracks, as shown in figure 12.

Acknowledgements

The authors are thankful to Professor Pierre Niay and Professor Marc Douay from Laboratory Physique des Lasers, Atomes et Molécules PhLAM at Lille University, for many useful discussions.

References

[1] Poumellec B, Niay P, Douay M and Bayon J F 1995 UV induced densification during Bragg grating writing *Photosensitivity and Quadratic Non-linearity in Glass Waveguides: Fundamentals and Applications* (Portland, USA: OSA)

[2] Sulimov V B, Sokolov V O, Dianov E M and Poumellec B 1995 Photoinduced structural transformation in silica glass: mechanism for UV written refractive index gratings *Photosensitivity and Quadratic Non-linearity in Glass Waveguides: Fundamentals and Applications* (Portland, USA: OSA)

[3] Cordier P, Dupont S, Douay M, Martinelli G, Bernage P, Niay P, Bayon J F and Dong L 1997 Evdience by transmission electron microscopy of densification associated to Bragg grating photoimprinting in germanosilicate optical fibres *Appl. Phys. Lett.* **70** 1204–6

[4] Douay M 1997 Densification involved in the UV-based photosensitivity of silica glasses and optical fibres *J. Lightwave Tech* **15** 1329–43

[5] Poumellec B, Niay P, Douay M and Bayon J F 1996 UV induced refractive index gratings in Ge:SiO_2 preforms: additional CW experiments and macroscopic origin of index change *J. Phys. D: Appl. Phys.* **29** 1842–56

[6] Gusarov A I, Doyle D B, Berghmans F and Deparis O 1999 Analysis of photoinduced stress distribution in fibre Bragg gratings *Opt. Lett.* **24** 1334–6

[7] Meltz G, Morey W M and Glenn W H 1989 Gratings in optical fibres by a transverse holographic method *Opt. Lett.* **14** 823–5

[8] Niay P, Bernage P, Legoubin S, Douay M, Xie W X, Bayon J F, Georges T, Monerie M and Poumellec B 1994 Behaviours of spectral transmissions of Bragg gratings written in germania-doped fibres: writing and erasing experiments using pulsed or CW UV exposure *Opt. Comm.* **113** 176–92

[9] Malo B, Johnson D C, Bilodeau F, Albert J and Hill K O 1993 Single-ecimer-pulse writing of fibre gratings by use of a zero-order nulled phase mask: grating spectral response and visualization of index perturbations *Opt. Lett.* **18** 1277–9

[10] Poumellec B and Kherbouche F 1996 The photorefractive Bragg gratings in the fibres for telecommunications *J. Physique III* **6** 1595–624

[11] Pironneau O 1996 FreeFEM—A language for the finite element method *Lab. d'analyse numérique Univérsité Paris 6*

[12] Poumellec B, Niay P, Douay M and Bayon J F 1996 The UV induced refractive index grating in Ge-SiO_2 preforms: additional CW experiments and the macroscopic origin of the change in index *J. Phys. D: Appl. Phys.* **29** 1842–56

[13] Chu P L and Whitbread T 1982 Measurement of stresses in optical fibre and preform *Appl. Opt.* **21** p 4241–5

[14] Limberger H G, Fonjallaz P Y, Salathé R P and Cochet F 1996 Compaction and photoelastic-induced index changes in fibre Bragg gratings *Appl. Phys. Lett.* **68** 3069–71

[15] Fonjallaz P Y, Limberger H G, Salathé R P, Cochet F and Leuenberger B 1995 Tension increase correlated to refractive-index change in fibres containing UV-written Bragg gratings. *Opt. Lett.* **20** 1346–8

[16] Atkins R M and Mizrahi V 1992 Observations of changes in UV absorption bands of singlemode germanosilicate core optical fibres on writing and thermally erasing refractive index gratings *Electron. Lett.* **28** 1743–4

[17] Williams D L, Davey S T, Kashyap R, Armitage J R and Ainslie B J 1992 Direct observations of UV induced bleaching of 240 nm absorption band in photosensitive germanosilicate glass fibres *Electron. Lett.* **28** 369–71

[18] Hosono H, Mizuguchi M, Kawazoe H and Nishii J 1996 Correlation between Ge E' centres and optical absorption bands in SiO2:GeO2 glasses *Japan. J. Appl. Phys. Lett.* **35** L234–6

[19] Leconte B, Xie W X, Douay M, Bernage P, Niay P, Bayon J F, Delevaque E and Poignat H 1997 Local Kramers–Kronig analysis of UV induced absorption changes: dynamics of excess loss induced by exposure to light at 248 nm or 193 nm in Ge:SiO_2 preforms *Bragg Gratings Photosensitivity, and Poling in Glass Fibres and Waveguides: Alications and Fundamentals* (Williamsburg, USA: OSA)

[20] Poumellec B, Guénot P, Riant I, Sansonetti P, Niay P, Bernage P and Bayon J F 1995 UV induced densification during Bragg grating inscription in Ge:SiO_2 preform *Opt. Mater.* **4** 441–9

[21] Janos M, Canning J and Sceats M G 1996 Incoherent scattering losses in optical fibre Bragg gratings *Opt. Lett.* **21** 1827–9

[22] Xie W X, Niay P, Bernage P, Douay M, Bayon J F, Georges T, Monerie M and Poumellec B 1993 Experimental evidence of two types of photorefractive effects occuring during photoinscriptions of Bragg gratings within germanosilicate fibres *Opt. Comm.* **104** 185–95